Compressed sensing reconstruction shortens the acquisition time for myocardial perfusion imaging: a simulation study

深見, 光葉

https://hdl.handle.net/2324/7182335

出版情報：Kyushu University, 2023, 博士（保健学）, 課程博士
バージョン：

Compressed sensing reconstruction shortens the acquisition time for myocardial perfusion imaging: A simulation study

Mitsuha Fukami[1),2)], Norikazu Matsutomo[1)], Takeyuki Hashimoto[1)], Tomoaki Yamamoto[1)], and Masayuki Sasaki[3)]

1) Department of Medical Radiological Technology, Faculty of Health Sciences, Kyorin University

2) Department of Medical Quantum Science, Graduate School of Medical Sciences, Kyushu University

3) Department of Medical Quantum Science, Faculty of Medical Sciences, Kyushu University

Mitsuha Fukami

Department of Medical Radiological Technology, Faculty of Health Sciences, Kyorin University

5-4-1 Shimorenjaku, Mitaka-shi, Tokyo 181-8612, Japan

Tel: +81-422-47-8000

E-mail: mitsuha-f@ks.kyorin-u.ac.jp

Norikazu Matsutomo, PhD

Department of Medical Radiological Technology, Faculty of Health Sciences, Kyorin University

5-4-1 Shimorenjaku, Mitaka-shi, Tokyo 181-8612, Japan

Tel: +81-422-47-8000

E-mail: nmatsutomo@ks.kyorin-u.ac.jp

Takeyuki Hashimoto, PhD

Department of Medical Radiological Technology, Faculty of Health Sciences, Kyorin University

5-4-1 Shimorenjaku, Mitaka-shi, Tokyo 181-8612, Japan

Tel: +81-422-47-8000

E-mail: hashi@ks.kyorin-u.ac.jp

Tomoaki Yamamoto, PhD

Department of Medical Radiological Technology, Faculty of Health Sciences, Kyorin University

5-4-1 Shimorenjaku, Mitaka-shi, Tokyo 181-8612, Japan

Tel; +81-422-47-8000

E-mail: tyamamoto@ks.kyorin-u.ac.jp

Masayuki Sasaki, PhD

Department of Medical Quantum Science, Faculty of Medical Sciences, Kyushu University

3-1-1 Maidashi, higashi-ku, Fukuoka-shi, Kyushu 812-8582, Japan
Tel: +81-92-642-6746
E-mail: sasaki.masayuki.165@m.kyushu-u.ac.jp

Abstract

Introduction: Compressed sensing (CS) has been used to improve image quality in single-photon emission tomography (SPECT) imaging. However, the effects of CS on image quality parameters in myocardial perfusion imaging (MPI) have not been investigated in detail. This preliminary study aimed to compare the performance of CS-iterative reconstruction (CS-IR) with filtered back-projection (FBP) and maximum likelihood expectation maximization (ML-EM) on their ability to reduce the acquisition time of MPI.

Methods: A digital phantom that mimicked the left ventricular myocardium was created. Projection images with 120 and 30 directions (360°), and with 60 and 15 directions (180°) were generated. The SPECT images were reconstructed using FBP, ML-EM, and CS-IR. The coefficient of variation (CV) for the uniformity of myocardial accumulation, septal wall thickness, and contrast ratio (Contrast) of the defect/normal lateral wall were calculated for evaluation. The simulation was performed ten times.

Results: The CV of CS-IR was lower than that of FBP and ML-EM in both 360° and 180° acquisitions. The septal wall thickness of CS-IR at the 360°acquisition was inferior to that of ML-EM, with a difference of 2.5 mm. Contrast did not differ between ML-EM and CS-IR for the 360° and 180° acquisitions. The CV for the quarter-acquisition time in CS-IR was lower than that for the full-acquisition time in the other reconstruction methods.

Conclusion: CS-IR has the potential to reduce the acquisition time of MPI.

Keywords: compressed sensing, myocardial perfusion image, acquisition time reduction, reconstruction methods, total variation

1. Introduction

Myocardial perfusion imaging (MPI) has been used as a diagnostic tool for the assessment of myocardial ischemia and infarction [1]. In particular, it has made a great contribution in predicting patient prognosis and short- and long-term risks of cardiac events [2]. However, the MPI examination requires an overall acquisition time of 20-30 min. Maintaining a supine position for such a long time may be burdensome for elderly patients, and motion artifacts generated during the examination can cause deterioration of the image quality of MPI. Consequently, MPI examinations may not be completed in all cases.

Compressed sensing (CS) has recently emerged as a technique for sparse computed tomography (CT) and magnetic resonance (MR) images. CS is used for recovering signals from undersampled images. Lustig et al. reported that the contrast of blood vessels on contrast-enhanced 3D angiography was *preserved at an acceleration of 20-fold when using CS reconstruction [3]. Jin et al. applied CS for assessing the soft tissue reconstruction process in sparse-view CT imaging and observed a small streak artifact in comparison with conventional filtered back-projection (FBP) [4]. CS has also been applied for single-photon emission tomography (SPECT) imaging [5]. The total variation (TV) based on CS was used for the sparsifying transform in the iterative process [6]. Panin et al. reported that TV was implemented as an L1-norm minimization method in maximum-likelihood expectation maximization (ML-EM) [7]. The TV reconstruction method has been reported to reduce noise while preserving the edge without a post-filter. However, the effect of CS, including TV, on image quality parameters, such as uniformity, spatial resolution, and detectability, of MPI has not been investigated in detail. CS is also expected to be useful in preserving image quality and thereby reduce the acquisition time with MPI. This preliminary study aimed to evaluate the performance of CS-iterative reconstruction (CS-IR) in comparison with those of FBP and ML-EM to reduce the acquisition time of MPI.*

2. MATERIALS AND METHODS

2.1 Digital phantom

The numerical digital phantom was generated by the Prominence Processor (Japanese Society of Radiological Technology), which is a simulation software program for SPECT imaging [8]. The phantom mimicked the left ventricular myocardium in the body with and without myocardial infarction in the lateral wall (Fig. 1). The size of the myocardial infarction was 2.8 cm^2. The pixel value for the soft tissue and defect area was 10, and that for the normal myocardium was 100.

2.2 Generation of projection data

The projection data were generated using the Prominence Processor. For the 360° acquisition, projection images with 120 (Full$_{360}$) and 30 directions (Quarter$_{360}$) were generated. For the 180° acquisition, projection images with 60 (Full$_{180}$) and 15 directions (Quarter$_{180}$) were generated. The 180° acquisition started at 225° followed by clockwise rotation to 45°. The pixel size was 3.2 mm × 3.2 mm. The rotation radius was 250 mm. The projection data were simulated using 20 kcounts/projection (equivalent to 20 s/projection with 740 MBq/mL administration). Additive statistical noise on the projection was randomly set for each dataset. In this study, attenuation, scattering and, degradation of spatial resolution by the collimators of photons was not considered. The simulation were performed ten times.

2.3 Image reconstruction

The MPI images were reconstructed using FBP, ML-EM, and CS-IR. A ramp filter was used for FBP. ML-EM was used for the iterative reconstruction methods according to the following formula:

$$\lambda_j^{(k+1)} = \frac{\lambda_j^{(k)}}{\sum_i C_{ij}} \sum_i \frac{y_i}{\sum_{j'} C_{ij'} \lambda_{j'}^{(k)}} C_{ij}$$

For CS-IR, images were reconstructed using IR with TV regularization. CS-IR was performed using the following formula [7].

$$\lambda_j^{(k+1)} = \frac{\lambda_j^{(k)}}{\sum_i C_{ij}\left\{1+\beta\frac{\partial}{\partial \lambda_j} U_{TV}\left(\lambda^{(k)}\right)\right\}} \sum_i \frac{y_i}{\sum_{j'} C_{ij'} \lambda_{j'}^{(k)}} C_{ij}$$

where i and j are the i^{th} pixel number in the detector and j^{th} pixel number in reconstructed image, respectively, k is the number of the iterations, λ^j is the value of image pixel j, y^i is the value of projection pixel i in the detector, Cij is the contribution from image pixel j to projection bin i, U^{TV} is the TV norm using the differential between a two pixel of 2D images, and β is the regularization parameter. The β value is a parameter for regularization involved in smoothing and conservation with an edge. The TV norm was evaluated as follows:

$$U_{TV} = \sum_{j,l} \sqrt{\left(\lambda_{j+1,l} - \lambda_{j.l}\right)^2 + \left(\lambda_{j,l+1} - \lambda_{j.l}\right)^2 + \varepsilon^2}$$

where j and l are the j^{th} pixel number for the x direction and l^{th} pixel number for the y direction, respectively. The number of iterations was 100, which was determined by coefficient of variation (CV), contrast ratio (Contrast) and septal wall thickness values in pre-experiments, i.e., CV, Contrast and the septal wall thickness was converged with 100 iterations. A Butterworth filter was used for preprocessing with an order of 8 and a cutoff frequency of 0.60 cycles/cm for FBP and ML-EM and 0.70 cycles/cm for CS-IR [9]. The parameters of the Butterworth filter were determined by the pre-experiments in which NMSE, CV, and the septal wall thickness were evaluated. The CS-IR reconstruction program was built in C programming language and the programing environment was a computer with configuration Intel (R) Core (TM) i5-9400 CPU @ 2.90GHz, 16 GB RAM, and GPU NVIDIA GeForce GTX 1650 with 4.0 GB dedicated GPU memory. The reconstruction time with FBP, ML-EM, and CS-IR were≤1 sec, 6.4 sec and 6.3 sec per slice, respectively.

2.4 Image analysis

The regions of interest (ROIs) are shown in FIGURE 1. The ROI_{heart} comprised the entire myocardium. ROI1 and ROI2 comprised the normal myocardium and lateral wall defects, respectively (Fig. 1). The total number of ROIs was five. ROI1 and ROI2 were circular and consisted of 12 pixels.

The CV of normal myocardium was calculated to evaluate the uniformity of myocardial *accumulation as follows:*

$$CV = \frac{SD_{ROI\ heart}}{MEAN_{ROI\ heart}}$$

where $MEAN_{ROI\ heart}$ is the mean count per pixel in ROI_{heart} and $SD_{ROI\ heart}$ is the standard deviation of the count per pixel in ROI_{heart}. septal wall thickness was calculated with the full width at half maximum (FWHM) to evaluate the influence of spatial resolution for the degradation [10]. The FWHM was calculated using the linear profiles perpendicular to the septal wall.

The Contrast of the defect and normal myocardium was calculated using the following formula to evaluate the detectability of the defect in the lateral wall:

$$Contrast = \frac{MEAN_{ROI1}}{MEAN_{ROI2}}$$

where $MEAN_{ROI1}$ and $MEAN_{ROI2}$ were the mean counts per pixel in ROI1 and ROI2.

2.5 Determination of the optimal β value

The appropriate β value for CS-IR was determined experimentally while balancing the uniformity and resolution. The MPI image was reconstructed with a β value ranging from 0.001 to 0.1 without any prefilter. The appropriate β-value for CS-IR was determined based on the CV results, the septal wall thickness, and normalized mean squared error (NMSE).

$$NMSE = \frac{\sum\sum(Target\text{-}Base)^2}{\sum\sum(Base)^2}$$

where "Target" was a reconstructed image with various β values and "Base" was a digital phantom image.

2.6 Statistical analysis

All results were expressed as the mean ± standard deviation. The Tukey–Kramer test was used for the statistical analysis of CV, septal wall thickness, and Contrast among the reconstruction methods. The Wilcoxon signed-rank test was used to compare the CV, the septal wall thickness, and Contrast between Full and Quarter images. P values < 0.05 were considered statistically significant.

3. Results

3.1 Determination of the optimal β value

The CV, septal wall thickness values, and NMSE with the 360°acquisition by different β value are shown in Table 1. The CV and NMSE decreased with increasing β values and then increased gradually. The lowest CV was obtained with a β value of 0.04 for the 360°acquisition and 0.05 for the 180°acquisition. The lowest NMSE was obtained with a β value of 0.03 for the 360°acquisition and 0.05 for the 180°acquisition. The septal wall thickness continuously increased with increasing β values. Finally, the optimal β value was determined to be 0.03 for the 360°acquisition and 0.05 for the 180°acquisition.

3.2 Image quality of normal myocardium

The CV and the septal wall thickness with the 360° acquisition by different reconstruction methods are shown in FIGURE 2. The CV with CS-IR (0.133 ± 0.006) was significantly lower than that with FBP (0.222 ± 0.003) and ML-EM (0.24 ± 0.008) ($P < 0.05$). Conversely, the septal wall thickness with CS-IR (16.5 ± 0.6 mm) was significantly inferior to that with FBP (14.9 ± 0.5 mm) and ML-EM (14.0 ± 0.5 mm) ($P < 0.05$). The difference in the septal wall thickness between CS-IR and ML-EM was 2.5 mm. The CV and the septal wall thickness with 180° acquisition by different reconstruction methods are also shown in FIGURE 2. The results with the 180° acquisition were similar to those obtained with the 360° acquisition. The difference in the septal wall thickness between CS-IR and ML-EM was 2.6 mm.

3.3 Detectability of the defect area in the myocardium

The Contrast obtained with different reconstruction methods is shown in FIGURE 3. In the 360° acquisition, the Contrast obtained with FBP was significantly higher than those obtained with ML-EM and CS-IR. The Contrast obtained with FBP, ML-EM, and CS-IR was 0.16 ± 0.02, 0.11 ± 0.02, and 0.12 ± 0.01, respectively. In the 180° acquisition, the Contrast obtained with FBP, ML-EM and CS-IR was 0.15 ± 0.03, 0.11 ± 0.03, and 0.12 ± 0.03, respectively. The results with the 180° acquisition were similar to those obtained with the 360° acquisition. However, the standard deviation with the 180° acquisition was larger than with the 360° acquisition.

3.4 Image quality and reduction in acquisition time

The image comparison between the Full and Quarter conditions is shown in FIGURE 4. Both $Full_{360}$ and $Full_{180}$, showed homogeneous distributions with FBP, ML-EM, and CS-IR. In $Quarter_{360}$ and $Quarter_{180}$, streak artifacts were observed in the background of the FBP image. In addition, a heterogeneous distribution of normal myocardium was observed in $Quarter_{360}$ and $Quarter_{180}$ with FBP and ML-EM. Further deterioration of uniformity was observed in $Quarter_{180}$ with FBP and ML-EM. On the other hand, images with CS-IR were superior in uniformity to those with other reconstruction method. However, the myocardial wall thickness with CS-IR was thicker than those with other reconstruction methods.

Comparisons of CV, septal wall thickness, and Contrast between Full and Quarter conditions are shown in FIGURES 5 and 6. In MPI with 360° acquisition (FIGURE 5), the CV of $Quarter_{360}$ was significantly inferior to that of $Full_{360}$ with all reconstruction methods ($P < 0.05$). However, the CV in

$Quarter_{360}$ with CS-IR was lower than that in $Full_{360}$ with the other reconstruction methods. The septal wall thickness was not significantly different between $Full_{360}$ and $Quarter_{360}$ with FBP, ML-EM, and CS-IR. The Contrast in $Quarter_{360}$ was significantly higher than that in $Full_{360}$ with ML-EM ($P < 0.05$). The Contrast in $Quarter_{360}$ was significantly lower than that in $Full_{360}$ with FBP ($P < 0.05$). The standard deviation of the FBP was larger than that of the other reconstruction methods in $Quarter_{360}$. However, the Contrast in $Quarter_{360}$ with CS-IR was not significantly different from that in $Full_{360}$ with CS-IR.

In MPI with 180° acquisition (FIGURE 6), the CV in $Quarter_{180}$ was significantly inferior to that in $Full_{180}$ for all reconstruction methods ($P < 0.05$). The CV in $Quarte_{180}$ with CS-IR was lower than that in $Full_{180}$ with the other reconstruction methods. The septal wall thickness showed no significant difference between $Full_{180}$ and $Quarter_{180}$ with all reconstruction methods. The Contrast in $Quarter_{180}$ was significantly higher than that in $Full_{180}$ with ML-EM ($P < 0.05$). The Contrast in $Quarter_{180}$ was not significantly different from that in $Full_{180}$ with FBP and CS-IR. However, the standard deviation of the FBP was larger than that of the other reconstruction methods in $Quarter_{180}$.

4. Discussion

In this study, the optimal β value for MPI using CS-IR was investigated, and a β-value of 0.03 for 360°acquisition and 0.05 for 180°acquisition was considered to be optimal. The CV with CS-IR was significantly lower than that with FBP and ML-EM in both 360° and 180° acquisitions. The septal wall thickness with CS-IR in the 360° acquisition was significantly inferior to that with ML-EM, with a difference of 2.5 mm. Contrast was not significantly different between ML-EM and CS-IR with 360° and 180° acquisitions. The CV of images with a quarter-acquisition time was inferior to that of images with a full-acquisition time, especially in the 180° acquisition. However, the CV in $Quarter_{180}$ with CS-IR was superior to that in $Full_{180}$ with the other reconstruction methods. The septal wall thickness in the quarter-acquisition time did not differ from that at the full-acquisition time. The Contrast in the quarter-acquisition time was not inferior to that in full-acquisition time for CS-IR.

MPI with decreased noise was reconstructed using CS-IR with higher β values. Tang et al. reported that the β value was used to control noise during the CS reconstruction process [11]. In this study, the optimal β value was determined to be 0.03 and 0.05 with CS-IR. However, Matsutomo et al. used a β value of 0.005 to achieve sufficient image quality and quantification in dopamine transporter imaging [8]. The β value in our study was larger than that reported in their study because the striatum is a tiny tissue, and a small β value is required to obtain high-resolution images. Because the spatial resolution deteriorates when the β value is too large, the appropriate β value should be determined by maintaining an appropriate balance between image resolution and uniformity in each examination.

The CV with CS-IR was superior to that with the other methods. Ahn et al. examined the feasibility of using CS reconstruction for reducing artifacts in positron emission tomography images. The uniformity with CS reconstruction was superior to reconstruction without CS, which is in line with our *results [12].*

Matsutomo et al. evaluated the spatial resolution in FWHM using the line source phantom, they reported that the FWHM of CS-IR was inferior to that in ML-EM and FBP [8]. In our study, the septal wall thickness with CS-IR was significantly inferior to that with ML-EM, with a difference of 2.5 mm for 360° acquisition and 2.6 mm for 180°acquisition. The difference was considered to originate from the degradation of spatial resolution. Generally, partial volume effects arise from the degradation of spatial resolution, and it is possible that the contrast is changed [13]. In this study, Contrast was calculated the ratio of defect area count to background. Thus, the lower Contrast was superior to higher Contrast. However, no significant difference in Contrast was observed between ML-EM and CS-IR. This may be attributed to the fact that the images were smoothed with a preserving edge in the CS reconstruction [6]. Contrast is an important factor for detecting defect areas. Thus, CS-IR can be applied for MPI in clinical settings. On the other hand, the left ventricular ejection fraction for patients with a small heart changes depending on the matrix size and cutoff frequency of the Butterworth filter [14]. Thus, measurements of myocardial function using gated SPECT might be influenced by using CS-IR.

Generally, a reduction in acquisition time results in deterioration of image quality parameters such as uniformity [15]. In our study, the CV in Quarter was significantly inferior to that in Full with all reconstruction methods. However, the CV in Quarter with CS-IR was superior to that in Full with FBP and ML-EM. The defect area was clearly observed in all the Quarter images, and the Contrast was not significantly different between the Full and Quarter images with CS-IR. Thus, CS-IR was considered useful for reducing the acquisition time in MPI. In addition, technologies developed to improve image quality have been reported to reduce acquisition time. Caobelli et al. reported the usefulness of IQ-SPECT for reducing the acquisition time. LV wall thickness and Contrast for the defect area were conserved during the quarter-acquisition time [16]. Wide-beam reconstruction (WBR) is a reconstruction algorithm used for resolution recovery. Marcassa et al. compared FBP with the full-acquisition time and WBR with half-time acquisition and found no significant difference in contrast recovery and FWHM [17]. However, IQ-SPECT and WBR are vendor-specific systems used for resolution recovery. Furthermore, the differences in image quality were determined using multivendor resolution recovery software [18] Because CS-IR is a vendor-free software, any institution or person can use it to obtain identical results. In our study, streak artifacts were observed in the Quarter images with FBP but not in the those with CS-IR. The contrast in the Quarter images with FBP was changed and it was markedly improved because the dark-band area and the white-streak artifact area were observed at the streak artifact area. CS has also been used to eliminate streak artifacts with sparse images and metal [19, 20]. Thus, CS-IR was considered useful for eliminating streak artifacts and for reducing the acquisition time. In this study, the Contrast in $Quarter_{360}$ was significantly higher than that in $Full_{360}$ with ML-EM. The bias between full-projection and half-projection images was increased by a reduction in the acquisition time and number of projections [21]. Thus, the Contrast in $Quarter_{360}$ $Full_{360}$ with ML-EM was changed by the reduction of acquisition time.

This study had some limitations. First, image quality with CS-IR was evaluated using a simulation study without attenuation, scatter, and degradation of resolution. Generation of projection data, including attenuation, scatter, and degradation of resolution information should be investigated in future studies. Second, other imaging filter such as a Gaussian filter and non-local mean filter and the parameter for attenuation correction, scatter correction, and resolution recovery have not yet been examined in detail. Further examination is required to determine imaging filters and these parameter for CS-IR. Finally, this was a simulation study using digital phantoms. Thus, the usefulness of CS-IR for MPI should be investigated in future clinical studies.

5. Conclusion

In MPI, the uniformity of CS-IR was superior to that of ML-EM and FBP without any significant deterioration in contrast. In addition, no significant difference was observed in uniformity between the Full and Quarter images with CS-IR. Thus, CS-IR is considered to have the potential to reduce the acquisition time of MPI.

Declarations

Conflict of interest

The authors report no potential conflict of interest relevant to this study.

Ethical approval

This was a simulation study. Thus, it did not require informed consent or ethical approval.

Figure legends

Fig.1 Digital phantom of the left myocardium and regions of interest.

(a) Normal left ventricular myocardium, (b) left ventricular myocardium with lateral infarction, (c) ROI_{heart} *for the whole left ventricular myocardium, and (d) ROI1 for the defect in the lateral wall and ROI2 for the normal myocardium.*

*Fig.2 Comparison of CV and septal wall thickness in reconstruction methods with 360° and 180° acquisition. *:* $p < 0.05$*. The CV of CS-IR was significantly lower than that of FBP and ML-EM with both 360° and 180° acquisitions. The septal wall thickness of CS-IR was significantly inferior to that of FBP and ML-EM with both acquisitions.*

*Fig.3 Comparison of Contrast in reconstruction methods with 360° and 180° acquisition. *:* $p<0.05$*. In 360° acquisition, Contrast was not significantly different between ML-EM and CS-IR.*

Fig.4 MPI with full- and quarter-acquisition time in reconstruction methods. The images with 360° acquisition are shown on the upper row and those with 180° acquisition are shown in the lower row. Streak artifacts were observed in $Quarter_{360}$ *and* $Quarter_{180}$ *of the FBP. A heterogeneous distribution in the myocardium was observed in the Quarter of FBP and ML-EM.*

*Fig.5 Influence of acquisition time reduction on image quality with 360°acquisition. (a) CV, (b) septal wall thickness, and (c) Contrast. *:* $p < 0.05$*.*

The CV with $Quarter_{360}$ *was significantly inferior to that with* $Full_{360}$ *in ML-EM. The Contrast with* $Quarter_{360}$ *was not significantly inferior to that with* $Full_{360}$ *in CS-IR.*

*Fig.6 Influence of acquisition time reduction on image quality with 180° acquisition. (a) CV, (b) septal wall thickness, and (c) Contrast. *:* $p < 0.05$*.*

The CV with $Quarter_{180}$ *was significantly inferior to that with* $Full_{180}$ *in all reconstruction methods. The Contrast with* $Quarter_{180}$ *was not significantly inferior to that with* $Full_{180}$ *in CS-IR.*

Reference

1. *Pozzoli MMA, Salustri A, Sutherland GR, et al. The comparative value of exercise echocardiography and 99m Tc MIBI single photon emission computed tomography in the diagnosis and localization of myocardial ischemia. Eur Heart J. 1991;12:1293-1299.*
2. *Chang SM, Nabi F, Xu J, et al. The coronary artery calcium score and stress myocardial perfusion imaging provide independent and complementary prediction of cardiac risk. J Am Coll Cardiol. 2009;54:1872-1882.*
3. *Lustig M, Donoho D, Pauly JM. Sparse MRI: The application of compressed sensing for rapid MR imaging. Magn Reson Med. 2007;58:1182-1195.*
4. *Jin SO, Kim JG, Lee SY. Bone-induced streak artifact suppression in sparse-view CT image reconstruction. Biomed Eng Online. 2012;11:44.*
5. *Kanazawa M, Sasaya T, Hosokawa S. Effect of Total Variation Regularization in Bone SPECT Reconstruction from a Small Number of Projections. 2019 IEEE Nuclear Science Symposium and Medical Imaging Conference (NSS/MIC). 2019:1-3.*
6. *Rudin LI, Osher S, Fatemi E. Nonlinear total variation based noise removal algorithms. Physica D. 1992;60:259-268.*
7. *Panin VY, Zeng GL, Gullberg GT. Total variation regulated EM algorithm [SPECT reconstruction]. IEEE Transactions on Nuclear Science . 1999;46:2202-2210.*
8. *Matsutomo N, Fukaya K, Hashimoto T. Performance of compressed sensing-based iterative reconstruction for single-photon emission computed tomography from undersampled projection data: a simulation study in 123I-N-ω-fluoropropyl-2β-carbomethoxy-3β-(4-iodophenyl) nortropane imaging. Nuclear Medicine Communications. 2019;40:106-114.*
9. *Onishi H, Matsutake Y, Matsutomo N. Validation of optimal cut-off frequency using a Butterworth filter in single photon emission computed tomography reconstruction for the target organ: spatial domain and frequency domain. Humanity and Science. 2010;10:27-36.*
10. *Caobelli F, Kaiser SR, Thackeray JT, et al. IQ SPECT allows a significant reduction in administered dose and acquisition time for myocardial perfusion imaging: evidence from a phantom study. Journal of Nuclear Medicine. 2014;55:2064-2070.*
11. *Tang J, Nett BE, Chen GH. Performance comparison between total variation (TV)-based compressed sensing and statistical iterative reconstruction algorithms. Phys Med Biol. 2009;54:5781–5804.*
12. *Ahn S, Kim SM, Son J, et al. Gap compensation during PET image reconstruction by constrained, total variation minimization. Med Phys. 2012;39:589-602.*
13. *Soret M, Bacharach SL, Buvat I, et al. Partial-volume effect in PET tumor imaging. Journal of nuclear medicine. 2007;48:932-945.*
14. *Kakhki VRD, Sadeghi R. Gated Myocardial Perfusion SPECT in Patients With a Small Heart: Effect*

of Zooming and Filtering. Clinical Nuclear Medicine. 2007;5:404-406.

15. *DePuey EG, Gadiraju R, Clark J, et al. Ordered subset expectation maximization and wide beam reconstruction “half-time” gated myocardial perfusion SPECT functional imaging: a comparison to “full-time” filtered backprojection. Journal of Nuclear Cardiology. 2018;15:547-563.*
16. *Caobelli F, Kaiser SR, Thackeray JT. IQ SPECT allows a significant reduction in administered dose and acquisition time for myocardial perfusion imaging: evidence from a phantom study. Journal of Nuclear Medicine. 2014;55:2064-2070.*
17. *Marcassa C, Campini R, Zoccarato O. Wide beam reconstruction for half-dose or half-time cardiac gated SPECT acquisitions: optimization of resources and reduction in radiation exposure. Eur J Nucl Med Mol Imaging. 2011;38:499-508.*
18. *Hughes T, Celler A. A multivendor phantom study comparing the image quality produced from three state-of-the-art SPECT-CT systems. Nuclear medicine communications. 2012;33:663-670.*
19. *Hu Z, Zheng H. Improved total variation minimization method for few-view computed tomography image reconstruction. BioMedical Engineering OnLine. 2014;13:70.*
20. *Deng Z, Zhou Y, Zhang W, et al. Customized Total Variation Algorithm for Metal Artifact Reduction in Computed Tomography. Annu Int Conf IEEE Eng Med Biol Soc. 2021:3479-3482.*
21. *Shiri I , AmirMozafari Sabet K, Arabi H, et al. Standard SPECT myocardial perfusion estimation from half-time acquisitions using deep convolutional residual neural networks. Journal of Nuclear Cardiology. 2021;28:2761-2779.*

Table 1. Determination of the optimal β value

	360°			180°		
β-value	CV	septal wall thickness	NMSE	CV	septal wall thickness	NMSE
0.001	0.422	11.9	0.525	0.454	10.7	0.644
0.003	0.334	12.2	0.387	0.408	10.9	0.555
0.005	0.285	12.3	0.302	0.370	11.1	0.481
0.008	0.245	12.6	0.225	0.326	11.5	0.395
0.010	0.228	12.7	0.193	0.303	11.6	0.353
0.020	0.185	13.6	0.125	0.244	12.9	0.243
0.030	0.165	14.5	0.114	0.221	13.7	0.205
0.040	0.158	15.0	0.117	0.212	14.2	0.191
0.050	0.159	15.5	0.124	0.210	14.6	0.188
0.060	0.163	15.6	0.133	0.212	14.6	0.195
0.080	0.185	15.9	0.163	0.234	15.2	0.220
0.100	0.213	16.4	0.214	0.245	15.7	0.271

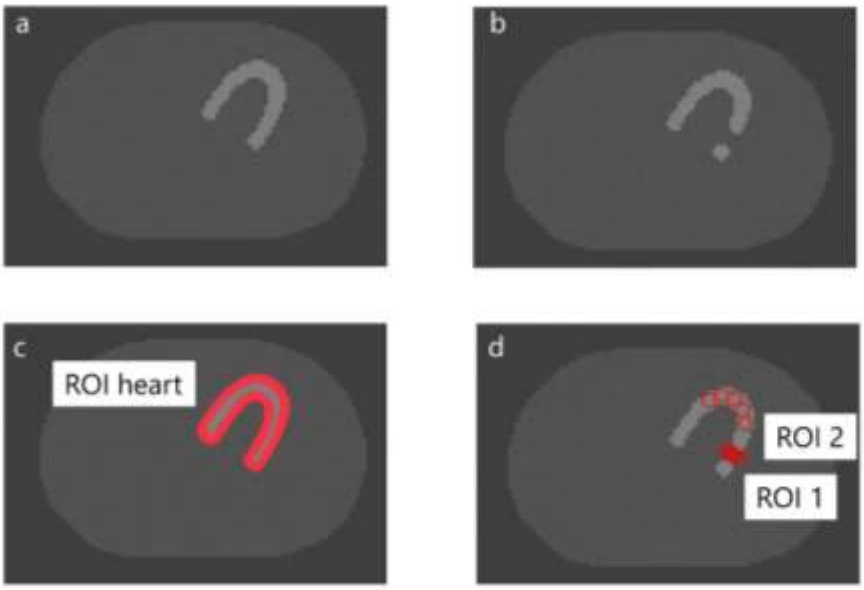

Fig.1 Digital phantom of the left myocardium and regions of interest.

(a) Normal left ventricular myocardium, (b) left ventricular myocardium with lateral infarction, (c) ROI_{heart} for the whole left ventricular myocardium, and (d) ROI1 for the defect in the lateral wall and ROI2 for the normal myocardium.

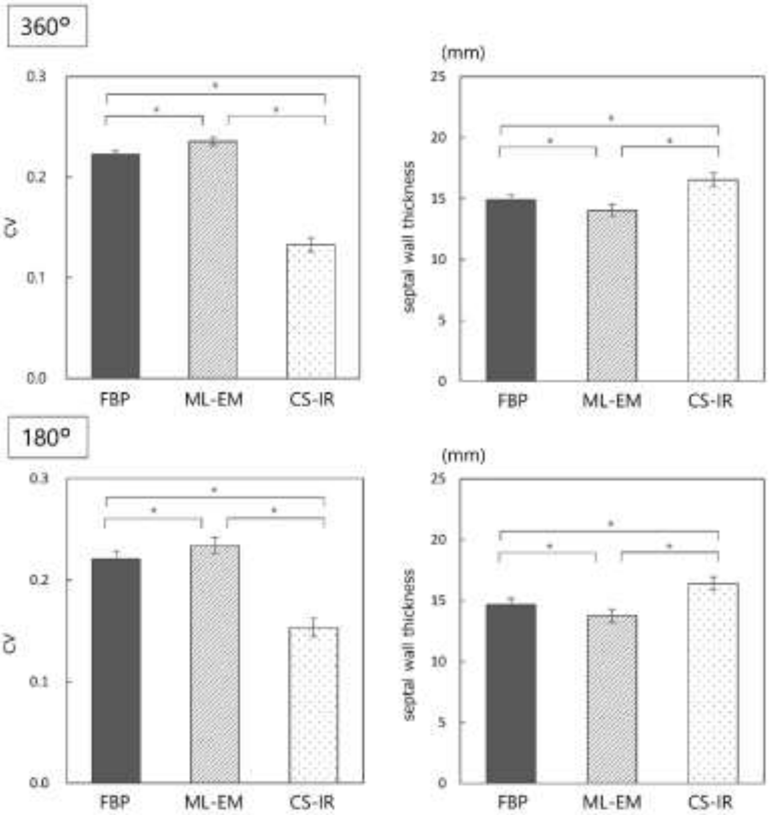

*Fig.2 Comparison of CV and septal wall thickness in reconstruction methods with 360° and 180° acquisition. *: p < 0.05. The CV of CS-IR was significantly lower than that of FBP and ML-EM with both 360° and 180° acquisitions. The septal wall thickness of CS-IR was significantly inferior to that of FBP and ML-EM with both acquisitions.*

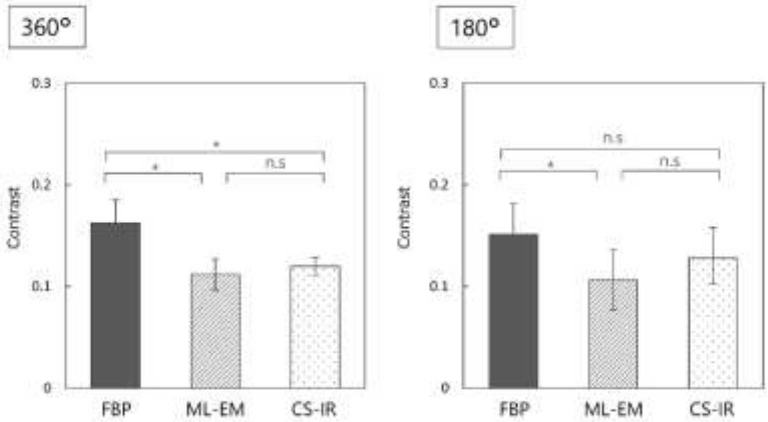

*Fig.3 Comparison of Contrast in reconstruction methods with 360° and 180° acquisition. *: p<0.05. In 360° acquisition, Contrast was not significantly different between ML-EM and CS-IR.*

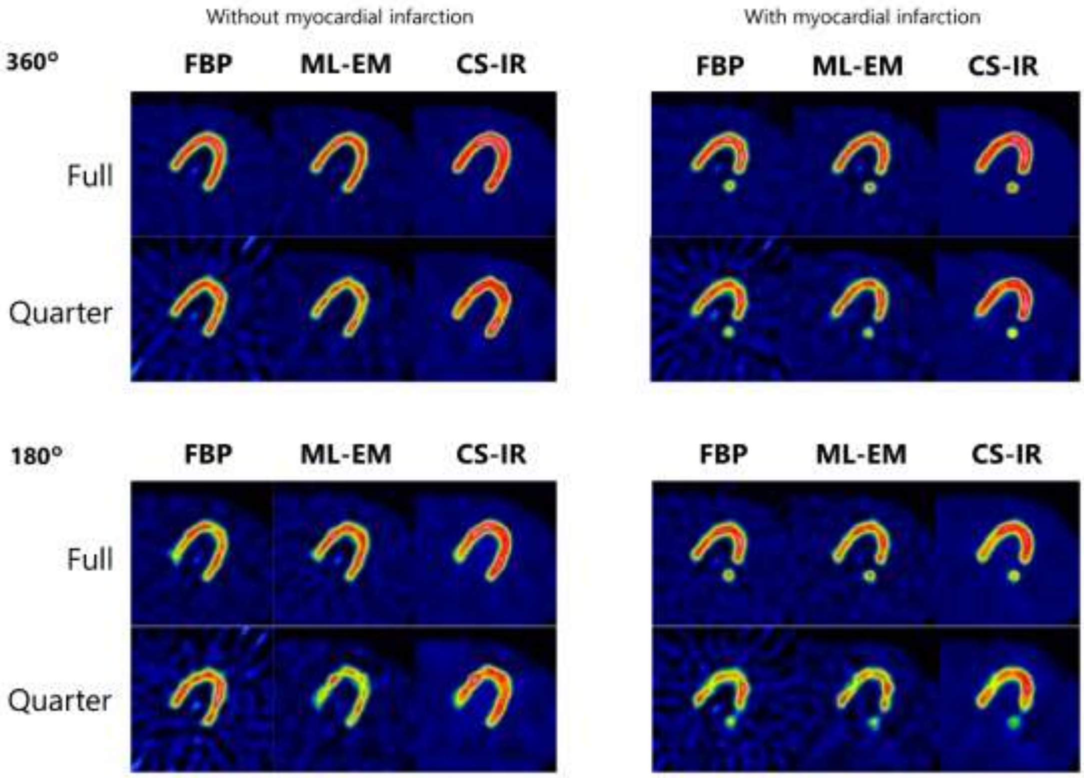

Fig.4 MPI with full- and quarter-acquisition time in reconstruction methods. The images with 360° acquisition are shown on the upper row and those with 180° acquisition are shown in the lower row. Streak artifacts were observed in Quarter$_{360}$ and Quarter$_{180}$ of the FBP. A heterogeneous distribution in the myocardium was observed in the Quarter of FBP and ML-EM.

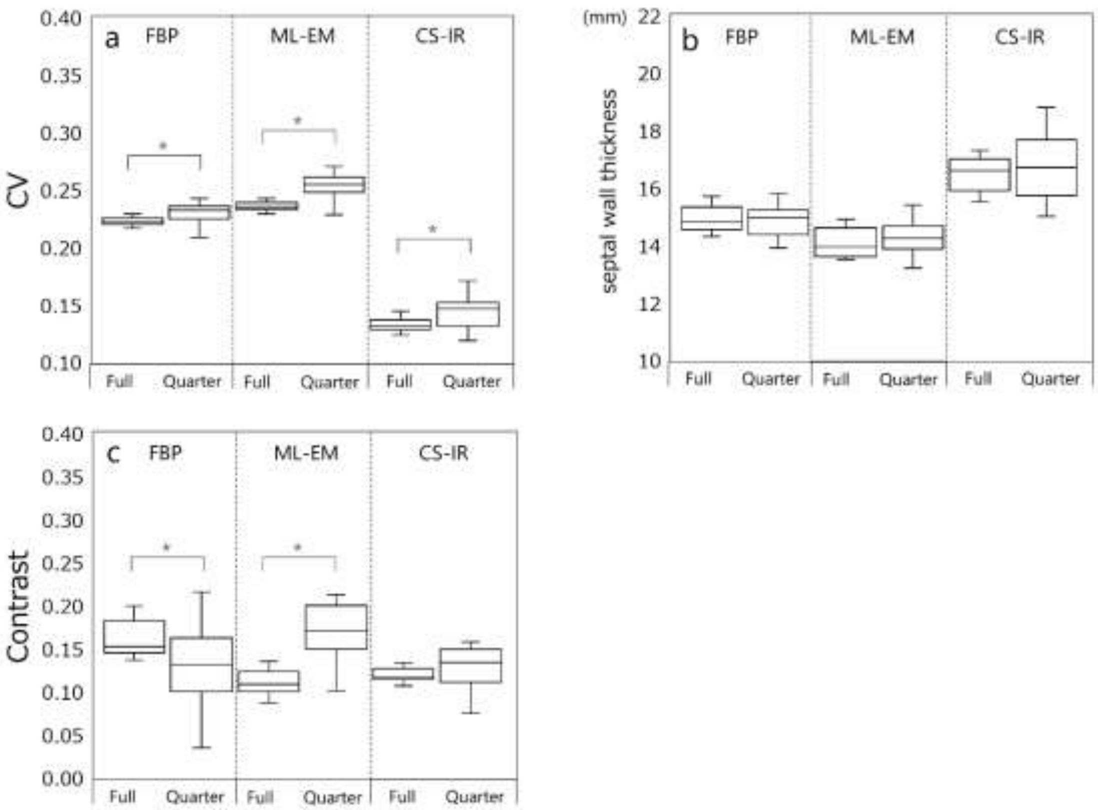

*Fig.5 Influence of acquisition time reduction on image quality with 360°acquisition. (a) CV, (b) septal wall thickness, and (c) Contrast. *: $p < 0.05$.*

The CV with $Quarter_{360}$ was significantly inferior to that with $Full_{360}$ in ML-EM. The Contrast with $Quarter_{360}$ was not significantly inferior to that with $Full_{360}$ in CS-IR.

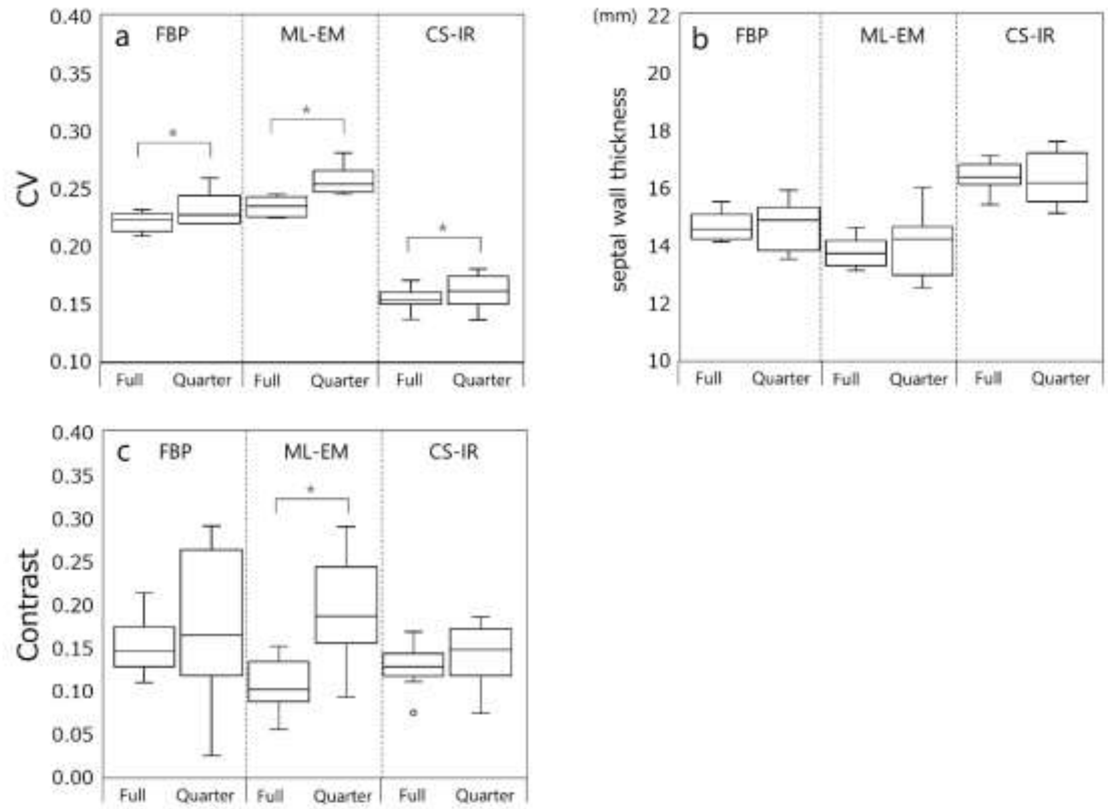

*Fig.6 Influence of acquisition time reduction on image quality with 180° acquisition. (a) CV, (b) septal wall thickness, and (c) Contrast. *: $p < 0.05$.*

The CV with $Quarter_{180}$ was significantly inferior to that with $Full_{180}$ in all reconstruction methods. The Contrast with $Quarter_{180}$ was not significantly inferior to that with $Full_{180}$ in CS-IR.